15
The Australian Remanent Anomalies Database as a precursor to a global database

C.A. Foss, P. Warren, P.W. Schmidt and S. Patabendigedara

ABSTRACT

We have developed the Australian Remanent Anomalies Database (ARAD) as a resource of magnetic field data, models and magnetisation direction estimates ascribed in part to remanent magnetisation. As far as we are aware, this is the first national database of magnetisation directions established from magnetic field data. ARAD is deployed in the AuScope Discovery web portal. In Australia there is restricted outcrop of fresh basement rocks and most rock magnetisations causing variation in the geomagnetic field are only known (with considerable associated uncertainty) from analysis or inversion of that magnetic field data. ARAD is designed as a location to store and search for magnetisation details. It supports download of any magnetic field data, models or magnetisation direction estimates that have been supplied for the database solutions.

Across large parts of Australia, FAIR (findable, accessible, interoperable and reusable) magnetic field data (https://ardc.edu.au/resource-hub/making-data-fair/) have been acquired and are distributed by Federal and State and Territory Governments. ARAD solutions are predominantly derived from these data, and a major objective for ARAD is to support analysis and interpretation of the same data. FAIR magnetic field coverage is increasingly available in many other countries, and we have included example solutions in ARAD from surveys beyond Australia. We have also included solutions derived from NOAA's global EMAG2 database (https://www.ncei.noaa.gov/products/earth-magnetic-model-anomaly-grid-2). Global and regional magnetic field compilations rely substantially on aeromagnetic data and the data quality and sufficiency of those surveys determines to what extent they support reliable recovery of magnetisation estimates from measured magnetic anomalies. Broad anomalies due to large crustal magnetisations produce fields that can be usefully analysed even from sparse and high-elevation magnetic field coverage, but smaller magnetisations that generate the majority of existing ARAD solutions are unresolved in present global magnetic field compilations.

The minimum requirement for an entry in the database is that key details are supplied of the anomaly and the survey in which it was measured. Close to magnetisations (in their 'proximal' fields) anomalies are of high amplitude but generally complex shape that creates challenges in estimation of magnetisation direction. Further from magnetisations (in their mid to far or 'distal' fields) estimation of the direction of magnetisation is less disrupted by the shape of distribution of magnetisation but isolation of these lower-amplitude anomalies is more problematic.

15.1 INTRODUCTION

The direction of magnetisation of a rock, whether known from laboratory measurement or from analysis and inversion of magnetic field data is of limited value without corresponding information from other rock units or magnetic anomalies. A key objective of the remanent anomalies database is to provide a context for analysis of magnetisation directions by comparison with directions from adjacent anomalies and/or palaeomagnetic measurements. Rocks acquire magnetisation during geological events such as the cooling of an igneous intrusion or metamorphic terrain through the blocking temperature range of its ferromagnetic grains or on sediment deposition and diagenesis. Complications arise from post-acquisition remagnetisation events and/or tectonic rotations that reorient magnetisation but under favourable circumstances directions of remanent magnetisation can also provide information about the timing and nature of that tectonism (Irving 1964; McElhinny 1973). In palaeomagnetism the requirement for multiple results that can be compared and combined was recognised long ago and there are published palaeomagnetic databases (Pisarevsky and McElhinny 2003; Pisarevsky 2005) and websites (Jarboe *et al*. 2012; Pisarevsky *et al*. 2022). Schmidt *et al*. (1990), Schmidt (2014) and Schmidt and Clark (2000) have reviewed palaeomagnetic data from Australia, and as more magnetisation directions are recovered from magnetic field analyses it will become increasingly productive to compare those directions with the palaeomagnetic data. Indirect determination of magnetisation from magnetic field data is particularly valuable in Australia where extensive cover and deep weathering restrict access for conventional palaeomagnetic sampling. Building a database of magnetisation directions from analysis of magnetic field data faces several additional challenges to creating a palaeomagnetic database: estimation of magnetisation from magnetic field data is indirect and uncertain, recovered magnetisation directions are the result of both induced and remanent magnetisation and the estimates depend on additional factors such as anomaly separation.

The Earth's magnetic field is a spatially continuous combination of the external fields of many different crustal magnetisations together with time-varying contributions from both the core and ionosphere. The magnetic field includes local variations (anomalies) different from the background field that arise from (anomalous) magnetisation different to the background magnetisation. Magnetic field anomalies are generally detected and defined visually in image, contour, magnetic profile or stacked profile displays. Anomaly separations are non-unique and require interpretive justification. Where anomalies cannot be visually recognised in a well-designed data display it is unlikely that magnetic field analysis or inversion can provide reliable results. Chapters 5 and 6 refer to 'sweet-spots' as segments of data that support analysis or inversion (in these cases for estimation of magnetisation direction). A single, discrete sweet-spot supports estimation of only a single, discrete magnetisation direction. However, multiple analyses or inversions can be applied to obtain different estimates of that direction and each of those alternate results can be entered into the database. All analytic and inversion techniques are based on similar assumptions about the nature and distribution of magnetisation and depend identically on validity of the input magnetic field data. Ability to cross-compensate for variation in estimated magnetisation direction with variation of other magnetisation parameters (particularly its horizontal location) means that even the most appropriate analysis or inversion of a well-defined sweet-spot leaves uncertainty in magnetisation direction greater than 5°. Voxel inversions are reported to recover multiple magnetisation directions across complete volumes of the sub-surface, but that level of detail cannot be justified and only a single magnetisation direction should be reported for each discrete magnetic field feature. Magnetic field variations that are indistinct or overlap extensively do not support meaningful recovery of magnetisation direction. ARAD accommodates quality factors and confidence levels that have been assigned to models and magnetisation direction estimates to guide their subsequent use. However, these statistics are only indicative (e.g. the 5° limit suggested above is an approximate estimate derived from sensitivity and repeatability analyses of measured and synthetic data).

A significant realisation that we came to early in construction of ARAD is that it is not helpful to think of a magnetic anomaly as primarily a feature of the magnetic field. A magnetic anomaly is only known by the measurements that express it and its primary definition must be with respect to those measurements. If a subsequent survey acquires new data at the same location then that new survey defines a new anomaly. The old anomaly remains valid and now has a new relationship to the more recent data with which it shares common sources. Also, an anomaly remains valid even if its source is

subsequently removed (e.g. by mining) and is no longer a feature of the present magnetic field. If we consider the hypothetical event of an instant reversal of the geomagnetic field, anomalies in the new field (that would need to be re-surveyed) could then with considerable advantage be related to the corresponding anomalies of quite different shape in the previous field to analyse pre- and post-reversal anomaly pairs with different induced magnetisation components and a common hard remanent magnetisation. This thought experiment highlights the concept that an anomaly belongs primarily to the survey data that defines it rather than being a fixed feature in the (continually changing) magnetic field.

The magnetic field measurements from which anomalies in the database are defined are almost exclusively of total magnetic intensity (TMI) made on aeromagnetic surveys. However, the database can also accommodate anomalies measured in ground or drone surveys and from vector component, field gradient or tensor data. These different magnetic field expressions are all directly related to each other and with sufficient data precision and distribution can be derived from each other (except for the indefinite integral in determination of a field from its gradients). ARAD allows that (with various advantages) models and magnetisation estimates can be derived from transforms and enhancements of the primary measured data. Examples of transforms include upward continuation of the field to higher elevation that reduces the influence of shape details in the distribution of magnetisation, and vertical derivatives to more effectively separate anomalies of interest from their background field.

Magnetic field anomalies are mostly due to local magnetisations stronger than the surrounding material, and in many cases much stronger. Magnetic field analysis and interpretation commonly assumes that the absolute magnetisation is identical to its contrast against surrounding magnetisation (i.e. that the background magnetisation is zero). Magnetisation estimates recorded in ARAD are almost exclusively of this effective (contrast) magnetisation but the values quoted as directions (declination and inclination) and strengths (A/m) or total magnetisations ($A.m^2$) can optionally include correction to absolute values against any independently known background value. From magnetic field images across many different geological settings it is evident that not all magnetic anomalies of interest are confidently separated from other overlapping field variations. In many cases geological processes result in complexity and variation within rock units that give rise to clusters of overlapping field variations. In such cases it is more challenging to isolate anomalies for analysis or inversion and it is also more difficult to justify the assumption that magnetisation contrast is a reliable estimate of absolute magnetisation.

Separation of an anomaly from its background field or overlapping fields of adjacent magnetisations is necessarily interpretive and should be supported by visual inspection to confirm that the results appear reasonable. Automated methods of anomaly detection and separation are convenient but must be supervised. The task is suitable for a comprehensively trained expert system but at the time of writing no such reliable system is available.

Where convenient, database entries include the sample of magnetic field data from which they were derived. These are in most cases of the supplied (processed TMI) data but optionally can be of data after a regional field separation or a transform such as the vertical derivative or upward continuation has been applied. In some cases the data are also supplemented with transforms such as the total gradient (also known as the analytic signal or modulus of the analytic signal) or normalised source strength (NSS). These transforms reduce the influence of magnetisation direction and provide approximate mapping of the horizontal distribution of magnetisation with reduced sensitivity to its direction. Data can be supplied in profile (mostly flightline) and/or grid format. The profile data are the more primary as grids create secondary data away from measurement locations. However, grid images are convenient for initial visual interpretations, and many processing operations are most conveniently performed by grid-based fast Fourier transforms (FFT). Note that magnetisation direction cannot be reliably resolved from analysis of single-channel data on a single profile. ARAD does not require specific data formats, but ESRI (ER Mapper) format with an easily read ASCII header file is encouraged for grids and ASCII or the widely used (but proprietary) Geosoft (GDB) format for profile data. Where data are provided for an anomaly they are packed in a zip file that can optionally include any other supporting information (that should be described by a simple 'readme' text file).

The intention when ARAD was first designed was that it would be made open for public submission of results and would grow by community contribution. Unfortunately, at present there are security issues in providing public access to externally populate ARAD and it is not feasible to allow direct public upload to it.

15.2 DESIGN OF THE DATABASE

Figure 15.1 is a simplified schematic of the database structure built around the central component of the anomaly list. The key relationships are that anomalies are generated by magnetisations controlled by geology and are detected and defined by surveys. The section of the database displayed in the upper half of Fig. 15.1 links geology to rock magnetic and palaeomagnetic studies. The geology is defined by geological events, geological ages and lithologies. This section of the database was designed to establish the fundamental relationships of the rocks carrying the magnetisations but to date it is only sparsely populated. Palaeomagnetic information is already provided in a global database that includes Australian data (Pisarevsky *et al.* 2022). There are benefits in having a single database source for palaeomagnetic data and so we have not proceeded to populate that section of the database. A future option is to link ARAD to an external palaeomagnetic database.

Few of the magnetic anomalies already in the database have samples from outcrop or drillhole available for palaeomagnetic or rock magnetic measurement. In north America and Scandinavia, recent glaciation has resulted in exposure of fresh samples of rock at surface and in those regions it is naturally more convenient to establish links between rock magnetism and the magnetic field. In Australia it is much more difficult to do this using only sparse drilling information. However, this restriction also raises the importance of the database as the only source of magnetisation information in some areas (albeit indirect and only of resultant magnetisation).

Database relationships mapped in the lower half of Fig. 15.1 are at present used much more extensively than those in the upper half. The linkage between anomalies and surveys is essential and the survey from which they are derived is a required statistic of all anomalies. At the time of writing all 300+ anomalies have at least one model. Previously, magnetic modelling results were disseminated in summary form in reports or publications available only to those aware of the studies and with access to the reports. ARAD models available for download from a web portal are much more publicly visible and accessible.

As a guide to considerations in building and using the database, the key elements of the surveys, anomalies, models and magnetisation estimate tables are shown in Table 15.1. Where feasible the element values are populated from drop-down options. Design of the database is a compromise between trying to ensure that all the information that is required and most of the information that is useful is collected, without the inconvenience of having to populate or navigate through rarely used options.

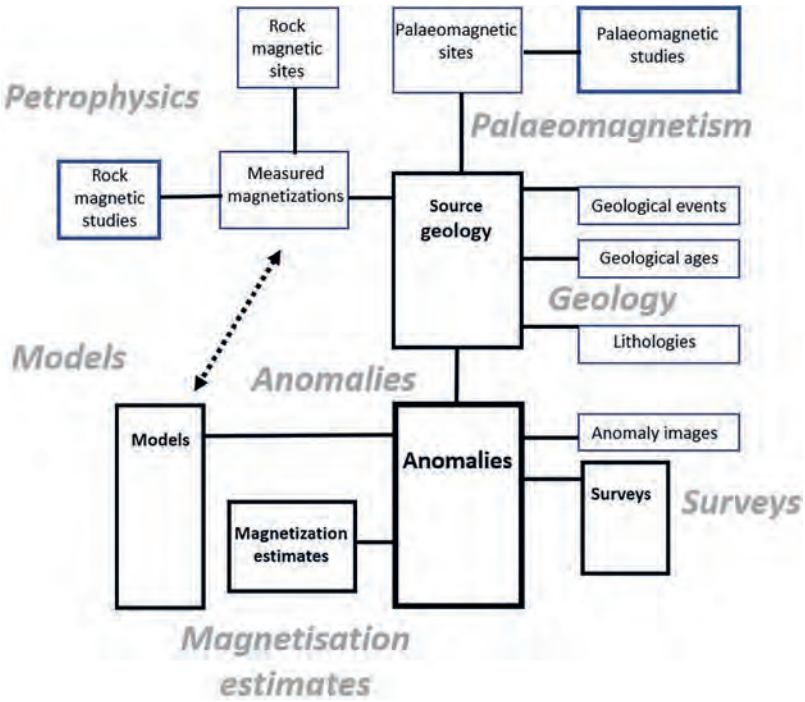

Fig. 15.1. Schematic of the database structure.

Table 15.1. Key anomaly database elements.

Surveys	Anomalies	Models	Magnetisation estimates	Magnetisation*
Survey ID	Anomaly ID	Model ID	Estimate ID	Known susc Y/N
Survey name	Anomaly name	Model name	Anomaly ID	Known remn Y/N
Database name	Survey ID	Anomaly ID	Estimation method	susceptibility
type	Geology ID	data type	Regional removal	Remanence int
year	data type	data derivation	centre	Remanence Dec
elevation type	data derivation	continuation ht	confidence	Remanence Inc.
ground clearance	continuation ht	data distribution	Analysis problem	Resultant int
single/multiline	longitude	model confidence	Continuation height	Resultant Dec
line spacing	latitude	model problem	Moment amplitude	Resultant Inc.
line orientation	IGRF Int/Dec/Inc.	Remanence Y/N	declination	Koenigsberger ratio
point spacing	extent N–S	Inversion Y/N	inclination	ARRA
area	extent E–W	model geometry	ARRA	
line km	+ve amplitude	spatial control	Optimisation stat	
highest elevation	−ve amplitude	elevation datum	Cluster statistic	
lowest elevation	shape	no. of bodies	Upload date	
data type	azimuth	top elevation	author	
E–W extents	data quality	depth below ground	comments	
N–S extents	data problem	volume		
outline filename	entry date	magnetisation*		
author	author	upload date		
comments	comments	author		
		comments		

15.3 DATABASE COMPONENTS

15.3.1 Surveys

The first action to upload an anomaly to the database is to locate the survey in the surveys list or to create a new survey entry. Anomalies cannot be entered into the database without being assigned to a survey. In Australia, Geoscience Australia maintain a survey database for the regional magnetic field data available from their GADDS (geophysical archive data delivery system) web portal (https://portal.ga.gov.au/persona/gadds). If the survey is in the Geoscience Australia survey database then the Geoscience Australia survey identifier (the project or 'P' number) is used but we also allow entry of surveys not in the GADDS register. The various survey parameters such as line spacing, terrain clearance and flightline direction all influence the definition of anomalies and the confidence with which magnetisation estimates can be derived.

15.3.2 Anomalies

The anomalies list is the core of the database. An anomaly is defined by survey data and is synonymous with a specific package of data. The unique specification of an anomaly is defined by the survey, geographic extents of the anomaly, data type, and any data transforms or continuation heights that have been applied. Transforms of the measured data, such as vertical derivatives or upward continuations define new anomalies. Also, if alternate flightlines are selected to investigate repeatability of results then each of the subsets of flightlines defines a separate anomaly. The versatility of this approach is required because an analysis or inversion only recovers information from the data submitted to it. Enhancements and transforms do not create new data but differentially weight the expression in the data of various parts of the magnetisation. By design, transforms and enhancements can focus on a magnetisation of interest but at the cost of possible distortion.

For some anomalies critical data might be missing. Misrepresentation of the magnetic field by undersampling is more problematic than is widely appreciated, possibly because grid images give the misleading suggestion that the magnetic field is continuously defined. Grid representation of a magnetic field is substantially

determined by the gridding algorithm that interpolates apparent data where none has been measured. If continuity of field curvature can be reasonably assumed between survey points or lines then advanced gridding algorithms such as those based on anisotropic diffusion (Naprstek and Smith 2019; Davis 2022) can be used with advantage over standard minimum curvature methods (Briggs 1974). These issues are considered in greater detail in Chapter 2. Chapter 10 considers the advantages of drone surveys flown at close line spacing to infill anomalies that have been detected but are insufficiently sampled by aeromagnetic surveys. Although the anomalies in both the aeromagnetic and drone surveys are generated by the same source magnetisation, different surveys provide different information about that magnetisation due to variations in their line spacing and flying heights.

15.3.3 Magnetisation estimates

There are several methods to estimate direction of magnetisation from magnetic field data (Clark 2014) including new methods presented in this book (Chapters 7 to 9). Two of the major approaches to estimation of magnetisation direction are those based on Helbig analysis (Helbig 1963; Phillips 2005; Foss and McKenzie 2011) and those investigating trial directions in correlation between transforms with low and high sensitivity to magnetisation direction (Fedi *et al*. 1994; Stavrev and Gerovska 2000; Dannemiller and Li 2006; Gerovska *et al*. 2009; Li *et al*. 2017; Liu *et al*. 2020). Magnetisation direction estimators are analyses designed to automatically recover estimates of magnetisation direction from magnetic field data without the need for inversion. The various methods each have different strengths and weaknesses but all have similar requirements for suitability of the input data. If data support reliable estimation of magnetisation direction by one method they will generally also support the alternative methods. None of the automated processes to estimate magnetisation direction have the versatility or reliability of a well performed and user-guided inversion. Magnetisation estimates are stored in the database together (optionally) with the data from which they are derived. Estimators of magnetisation direction will become more important when they are developed to the stage that they can provide sufficient resolution and reliability to define populations of anomalies with a common magnetisation direction. To be useful, the lower reliability of the estimates must be compensated by the ease of generating solutions in an automated or at least lightly supervised process. Ideally the solutions should include one or more quality factors that can be applied as a filter to reject less reliable solutions and to promote the more reliable solutions for verification and upgrade by inversion.

15.3.4 Models

Models, unlike magnetisation direction estimates, provide fully specified solutions from which a magnetic field (hopefully consistent with the input measured field) can be forward computed. A source model for any anomaly is optional and each anomaly can have multiple alternative models. A model is specified by the data from which it is derived, together with its key parameters. Models can be forward computed using a magnetisation direction from rock-magnetic measurement, magnetic field analysis or by specification. Alternatively (as is the case for most ARAD anomalies) models can be derived by inversion that discovers an estimate of magnetisation direction from the input data. Significant attention is paid through other chapters of this book (especially Chapters 1 and 5) to the non-uniqueness of models. Any model that conforms to independent constraints and produces an acceptable match to the input data (a subjective decision) is a candidate representation of the true magnetisation. The fields computed from models are added to associated background fields to match the measured field and this separation of fields is an essential aspect of any model.

To present, most ARAD anomalies have been isolated, modelled and inverted using ModelVision software (Pratt *et al*. 2020). These models are stored in the ModelVision (ASCII) 'tkm' format that includes magnetisation information and enables their further interrogation by modelling or inversion. The models are also stored in purely spatial 3D-DXF and Gocad T-surf formats for inclusion in GIS with other spatial models and data. Models derived using alternative software can also be uploaded to ARAD with the main requirement that each individual model body is characterised by and reported using a single magnetisation direction. Projections of the models are inherited from projection of the data from which they have been derived (that must be reported in the metadata).

15.4 THE DATABASE OF AUSTRALIAN MAGNETISATIONS

Figure 15.2 shows the distribution of ARAD solutions across Australia displayed in the AuScope web portal and

Fig. 15.2. ARAD solutions (300+) over a TMI image of Australia captured from the Geoscience Australia web portal.

Fig. 15.3 shows selection of anomaly 1 (the north-west Black Hill Norite anomaly) with buttons for download of the anomaly grid, models and images. Many of the ARAD solutions have been derived from the same data as the background TMI image or data of similar resolution, but some ARAD solutions are derived from higher resolution (but still publicly available) data with anomalies that may not be evident in the background image.

The 300+ Australian solutions currently in ARAD represent the more emphatic expressions of remanent magnetisation in the Australian magnetic field but these are only a minute selection of the total field variations, most of which have some contribution from remanent magnetisation. Although the prime objective of the database is to detail and map remanent magnetisation, ARAD also includes solutions with magnetisation parallel to the local geomagnetic field. We envisage the ideal future of the database as a record of all magnetisation estimates that can be recovered from the magnetic field. With improved understanding of the expression of magnetisation in the magnetic field data and how to optimise its recovery it is feasible that the number of ARAD solutions can be grown exponentially. We hope that there will also be continual upgrade of the magnetic field coverage from which new and improved magnetisation estimates can be derived. Just as with mining, where upgraded processes enable metal recovery from reprocessing of old mine tailings, it should be feasible to continually upgrade ARAD as analytic techniques and inversion procedures improve.

15.5 EXAMPLE DATABASE ENTRIES BEYOND AUSTRALIA

National borders need not limit the scope of ARAD. The database has been designed specifically for use with FAIR magnetic field data because solutions derived from proprietary data are not open to verification. FAIR magnetic field data is becoming increasingly available across the world and supports extension of ARAD or the

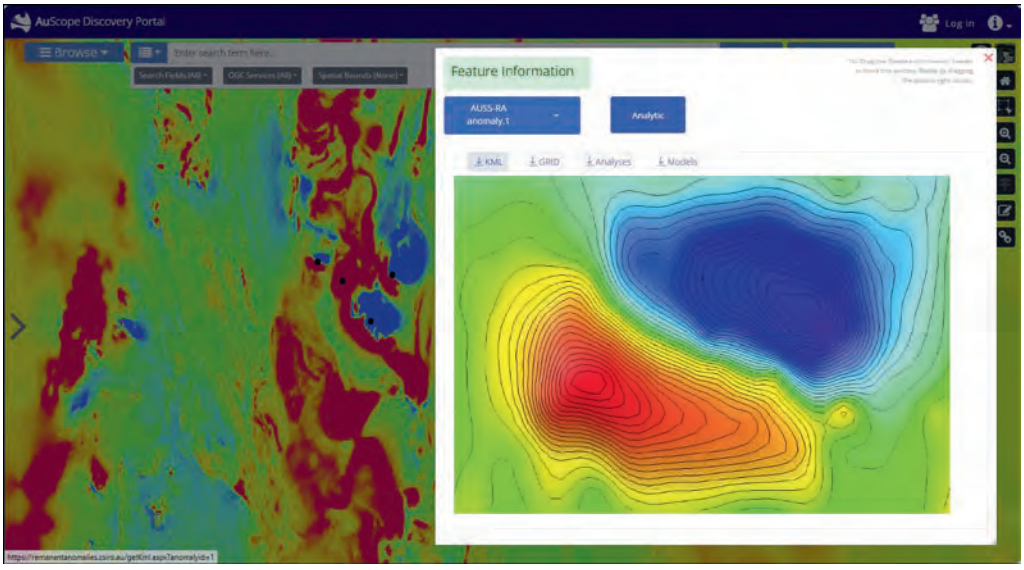

Fig. 15.3. AuScope portal zoom-in of the TMI and solutions in the vicinity of the ARAD001 solution from the Black Hill Norite of South Australia. The pop-up sidebar provide details of the anomaly with buttons to download a kmz image, a grid clip and models.

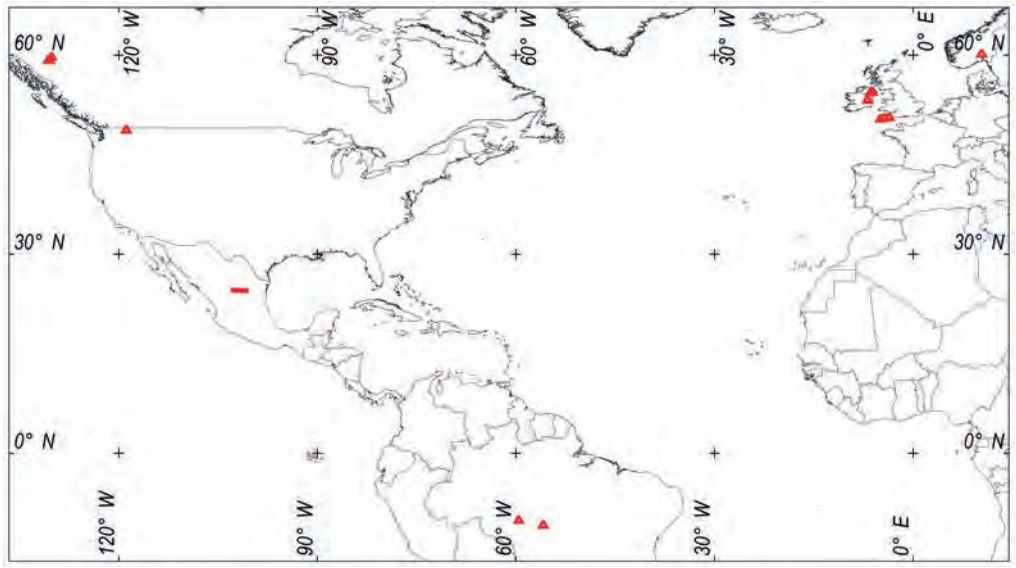

Fig. 15.4. Distribution of solutions beyond Australia as of March 2025.

Table 15.2. List of ARAD solutions outside Australia as of July 2024.

Anomaly	Country	Name	Longitude	Latitude	Description
313	Brazil	Caca_dos_Tapiunas	-59.60	-10.10	Intrusive
331	Brazil	Rio Claro	-55.89	-10.82	Wide circular sheet
332	Canada	Jennings_River ne	-130.18	59.72	Reverse magnetic plug
333	Canada	Jennings_River sw	-130.62	59.31	Reverse magnetic plug
334	Canada	Mathews Tuya	-130.43	59.19	Thin sheet
335	Mexico	El Puerto de la Palma	-102.71	24.58	Volcanic complex
336	Mexico	Los Chiqueros	-102.18	24.55	Volcanic complex
337	Mexico	El Cabresante	-101.46	24.61	Volcanic complex
338	Mexico	El Penuelo	-100.80	24.58	Volcanic complex
339	UK	Hennock	-3.66	50.61	Possible mineralisation
340	UK	Trewinnion	-4.98	50.38	Intrusive?
341	UK	Callington	-4.33	50.50	Intrusive?
342	USA	Clackamas Mtn NW	-118.91	48.73	Plug?
343	USA	Clackamas Mtn SE	-118.87	48.71	Plug?
344	Ireland	Broomhedge	-6.18	54.49	Reverse magnetic plug
345	Ireland	Clare	-6.48	54.32	Reverse magnetic plug
346	Ireland	Grange Common	-6.91	53.21	Two volcanic bodies?
347	Norway	Haugsbygd	10.34	60.19	Intrusive plug?

creation of equivalent databases in other regions. Here we present database entries generated beyond Australia to illustrate the benefits such a database provides in value-adding to the magnetic field data and hopefully ARAD will grow with new solutions both within and outside Australia. Figure 15.4 shows the March 2025 distribution of database solutions beyond Australia. Table 15.2 lists the anomalies and Table 15.3 provides key estimated statistics of the source magnetisations for those anomalies.

Table 15.3. Peak-Trough amplitudes of the anomalies in Table 15.2 and their magnetisation estimates.

Anomaly	Peak-Trough Amplitude (nT)	Model(s)	Intensity (A/m)	Magnetic Moment ($A.m^2.10^6$)	Declination	Inclination	ARRA
313	730	Elliptic pipe	40.46	49,890	336°	−54°	53°
331	732	Elliptic pipe	1.836	491,288	350°	+5°	11°
332	767	Elliptic pipe	8.29	846	255°	−85°	168°
333	443	Elliptic pipe	3.069	252	132°	−77°	165°
334	1,888	Polygonal pipe	11.20	6,317	300	+85°	14°
335	946	Elliptic pipe	45.49	1,258,400	357°	+64°	27°
336	807	Elliptic pipe	19.05	913,800	339°	+49°	25°
337	1,303	Elliptic pipe	24.42	2,107,500	25°	+52°	24°
338	1,762	Polygonal pipe	21.01	2,231,000	16°	+62°	28°
339	659	Elliptic pipe	6.77	62	178°	−20°	134°
340	91	Polygonal pipe	0.616	290	180°	−22°	137°
341	146	Elliptic pipe	7.87	159	191°	+27°	86°
342	1,736	Elliptic pipe	10.7	501	218°	−87°	164°
343	2,475	Elliptic pipe	54.6	210	165°	−64°	167°
344	745	Elliptic pipe	4.60	144	185°	−45°	156°
345	1,643	Elliptic pipe	19.5	212	224°	−68°	163°
346	267	Elliptic pipe	2.95	291	340°	+47°	21°
347	2,800	Circular pipe	35.95	638	190°	−31°	138°

15.5.1 Anomaly ARAD331, Brazil

Figure 15.5 shows a TMI anomaly measured by the Japuíra survey in the Mato Grosso region of Brazil. The data can be downloaded from the Geological Survey of Brazil geoscience system (https://geosgb.sgb.gov.br/geosgb/about_geosgb_en.html). The survey was flown on north–south flightlines at a line spacing of 500 m and a nominal terrain clearance of 100 m. Figure 15.5B shows the anomaly computed from inversion with a homogeneous horizontal-top, elliptic-section pipe model of average diameter of 14 km and depth extent 1,800 m. As shown by the similarity of the images in Fig. 15.5 A and 15.5B, the model matches the anomaly quite successfully. However, compromises in matching data over such a large area with a simple model mean that at any one location the model is an unreliable representation of the local in-ground magnetisation (e.g. of spot values of depth to the top of magnetisation). Figure 15.6 shows a profile extracted from the model along a central north–south flightline (note the data-fit is not derived exclusively on this flightline but on the complete flightline set). The high-amplitude, short-wavelength variations would cause considerable uncertainty for a model derived from single flightline data but there is effective cancellation of these irregularities over the large number of flightlines inverted. This stability of the model was confirmed by running inversions with the complete dataset, and with even- and odd-numbered flightlines only. All three inversion models returned very similar magnetisation estimates. The −5° geomagnetic inclination at the site was chosen as the starting model magnetisation direction, and the +5° post-inversion estimate of the inclination of magnetisation (an ARRA of 10°) is consistent with the tri-pole morphology of the anomaly with flanking positive lobes to both the north and south of the central low body as explained in Chapter 14.

15.5.2 Anomalies ARAD342, ARAD343 Clackamas Mountain, Washington State, USA

Figure 15.7 shows a segment of TMI measured by the Republic Survey flown for the United States Geological Survey (USGS) and Washington Department of Natural Resources as part of the Earth Mapping Resources Initiative (EMRI) in Washington State, USA (Staisch *et al.* 2024) (https://www.sciencebase.gov/catalog/item/65959be8d34e3265ab152eed). The survey was flown on flightlines at 200 m spacing and with a mean terrain clearance for the two anomalies

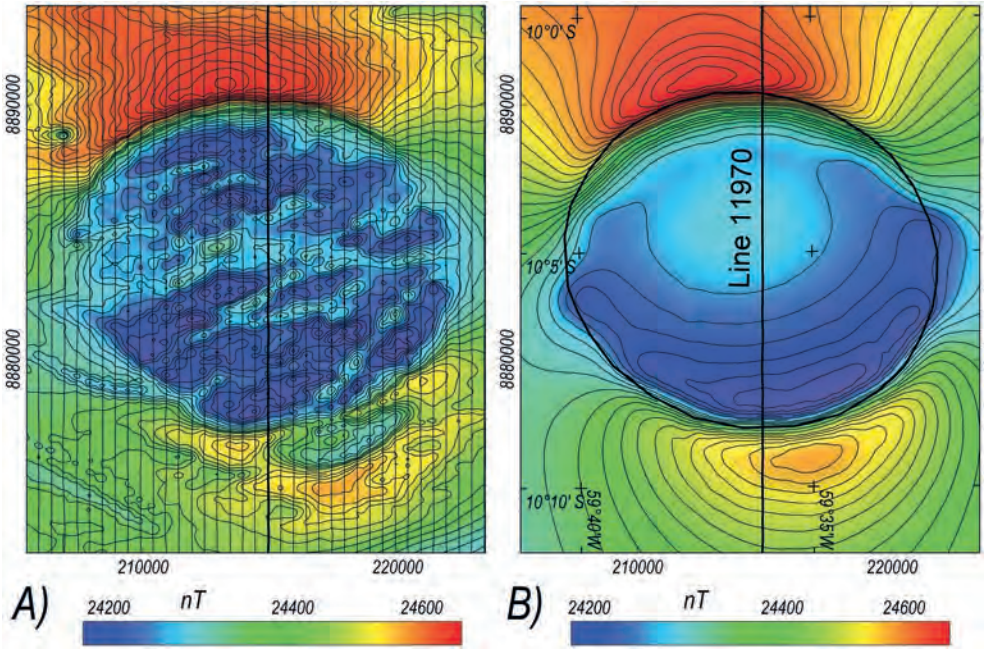

Fig. 15.5. A) measured and B) model-computed TMI for ARAD anomaly 331. The outline of the elliptic-section model is plotted in B). A section through the model along flightline 11970 is shown in Fig. 15.6.

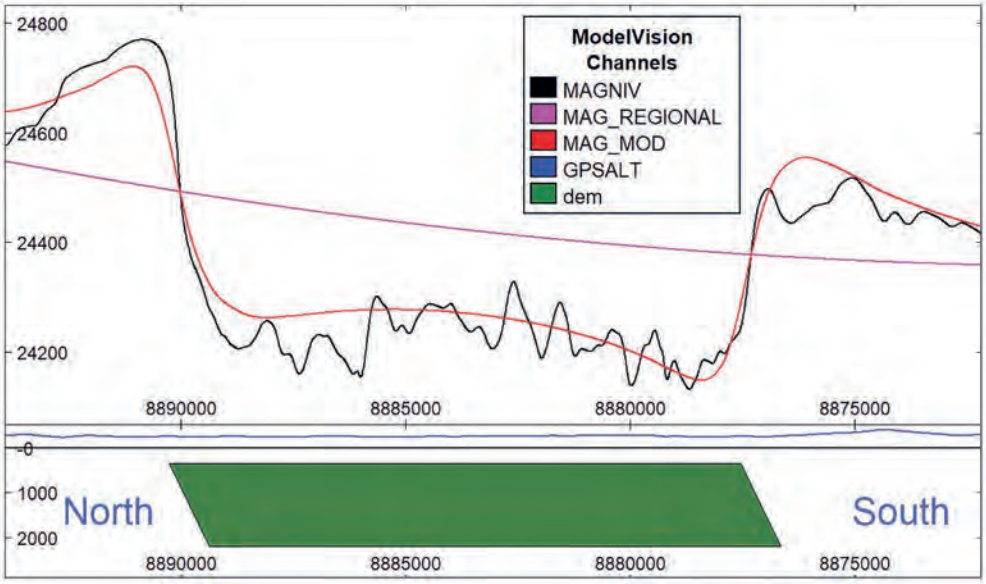

Fig. 15.6. North–south section along central flightline 11970 (for location see Fig. 15.5).

studied of 130 m. Figures 15.8A and 15.8B show anomalies ARAD342 and ARAD343 in more detail with overlays of the top of the elliptic-section pipe models generated to match them. Each anomaly, defined by five to six east–west flightline segments of approximately 1 km length, is composed of a prominent subcircular trough with a lower-amplitude peak to the north. The polarity of the anomalies is opposite to that expected of induced magnetisations at this latitude and suggests that they are due to reverse magnetisations. The ARRA values for the two anomalies are 167° and 164° (Table 15.3) compared to 180° for an exact reverse magnetisation. The anomalies are modelled with both plunging elliptic-section pipes (shown in red) and

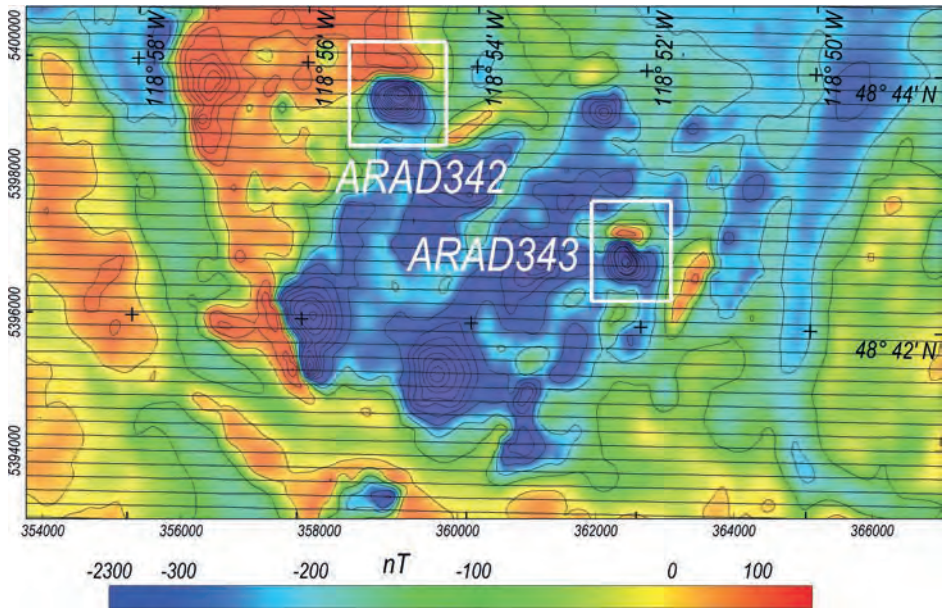

Fig. 15.7. Segment of TMI from the Republic Survey flown over Clackamas Mountain, including anomalies ARAD342 and ARAD343.

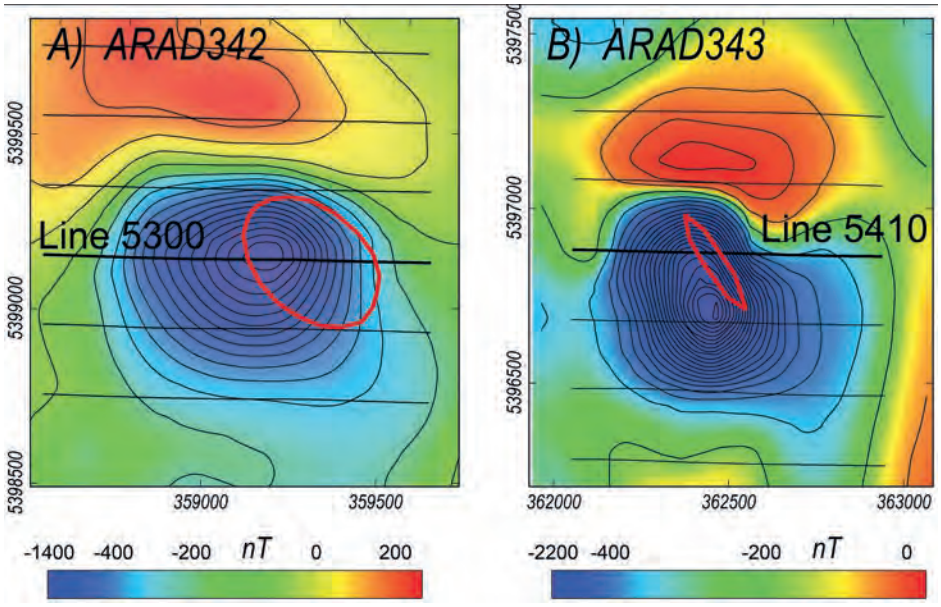

Fig. 15.8. TMI anomalies with east–west flightlines and outlines of the tops of inversion models for: A) ARAD342 and B) ARAD343.

ellipsoids (shown in blue). Sections through the inversion models along the central flightlines shown in Figs 15.9A and 15.9B reveal that the magnetisations are outcropping or very close to surface. Inversions with the two body types (independent other than they share the same input data and almost identical anomaly separations) give magnetisation directions with differences of only 3°and 8° for anomalies ARAD342 and ARAD343 respectively. Unfortunately, even for these probably outcropping magnetisations it is unlikely that palaeomagnetic measurement of remanent magnetisation (NRM) can be applied in modelling the anomalies because these prominent sites are likely to be heavily lightning struck. Nevertheless, it may be possible to determine the direction of remanent magnetisation with thermal or alternating-field demagnetisation.

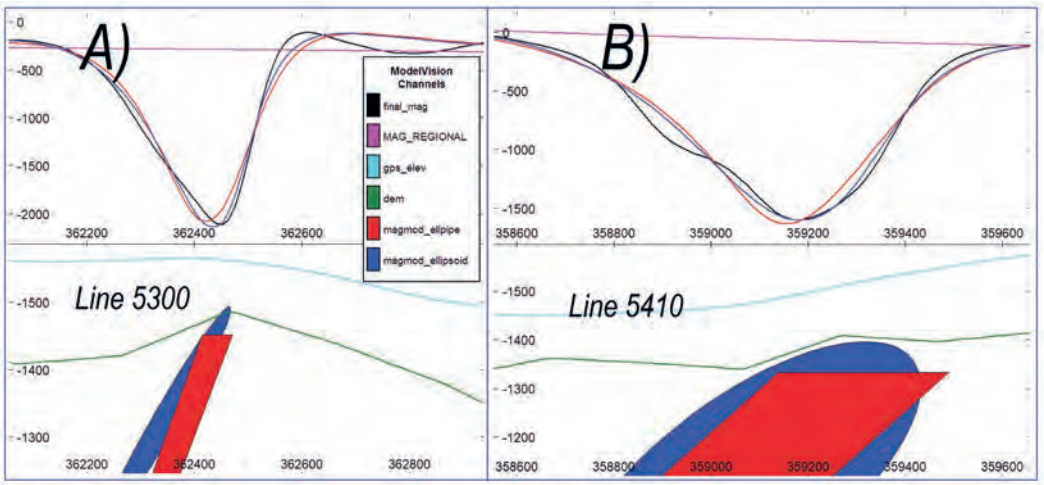

Fig. 15.9. Central west-to-east flightlines for A) Anomaly ARAD 342 and B) Anomaly ARAD343.

15.5.3 ARAD anomaly 334 over Matthews Tuya, British Columbia, Canada

Figure 15.10 shows a segment of TMI measured by the Jennings River Survey in northern British Columbia. The survey was flown on north-west-south-east flightlines at 500 m spacing and a nominal terrain clearance of 150 m. The data can be downloaded from the Natural Resources Canada website (https://osdp-psdo.canada.ca/dp/en/search/metadata/NRCAN-GEOSCAN-1-223258) or the Geoscience British Columbia website (https://www.geosciencebc.com/projects/2005-059/). The geomagnetic inclination of +76° at this site is steep and the almost single-signed negative amplitude anomalies ARAD332 and ARAD333 (Fig. 15.10) are due to magnetisations with similarly steep southerly inclinations (inversion results for these two anomalies are listed in Table 15.3). The predominantly positive anomaly over Matthews Tuya (anomaly ARAD334) is clearly due to a

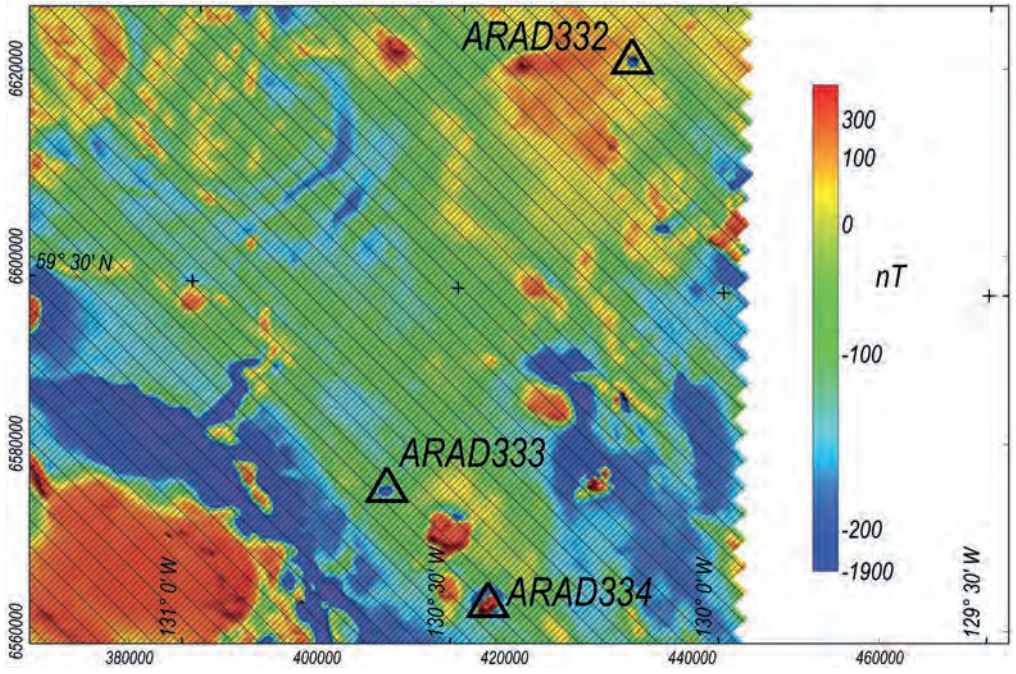

Fig. 15.10. Section of the Jennings River Survey in British Columbia including anomalies ARAD332, ARAD333 and ARAD334.

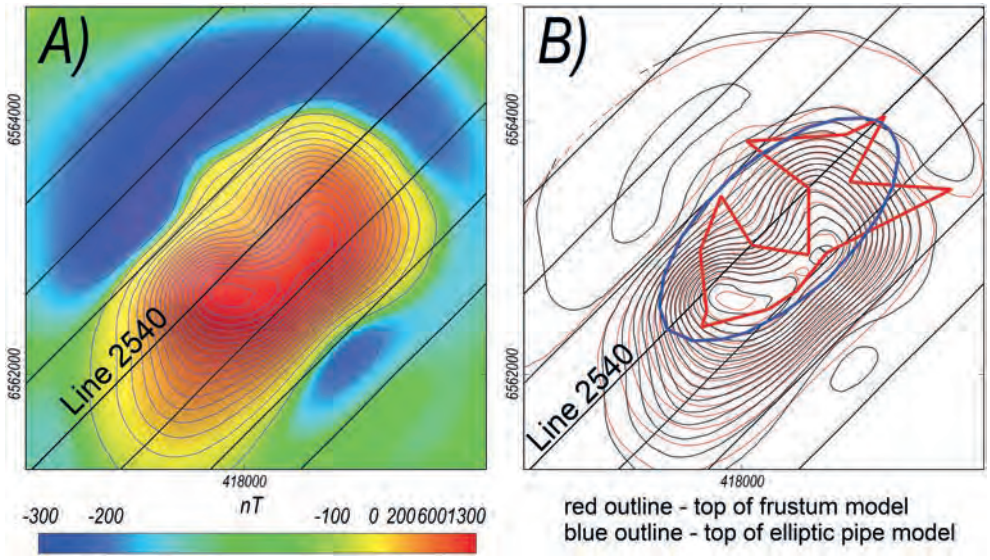

Fig. 15.11. A) TMI image and flightlines over Anomaly ARAD334 and B) measured (black) and computed from polygonal-section model (red) contours with outlines of the tops of the polygonal-section (red) and elliptic-section (blue) models.

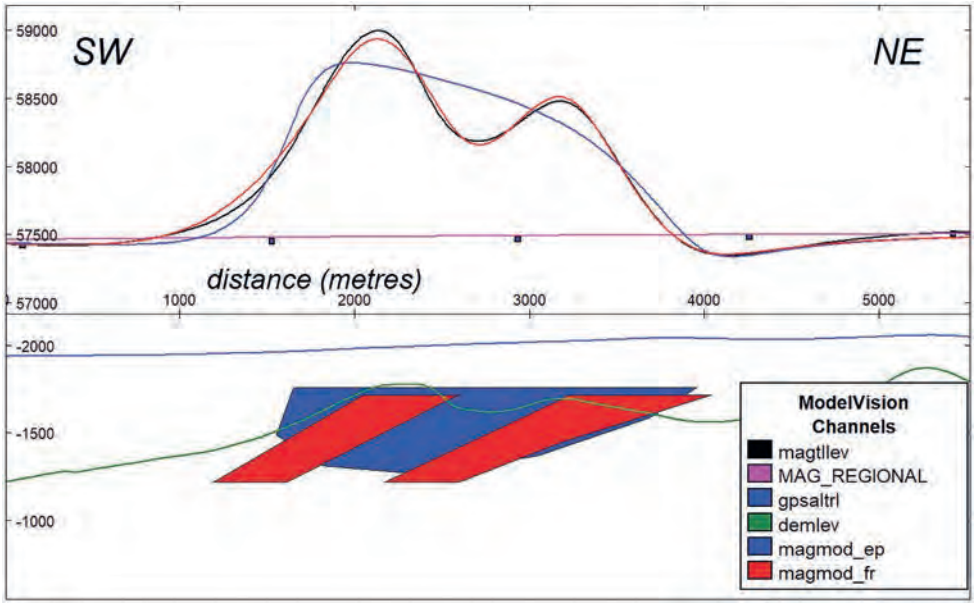

Fig. 15.12. Section along flightline 2540 with polygonal-section (red) and elliptical-section (blue) models.

quite different magnetisation, closer to the geomagnetic field direction. Figure 15.11A shows the measured anomaly over Matthews Tuya (a tuya is a flat-topped, steep-sided volcanic sheet erupted through a glacier or ice sheet). The anomaly is elongate in the south-west-north-east direction parallel to the flightline direction and is sampled on only two lines (each of which has very different expression of what is clearly a complex anomaly). We inverted the anomaly using both a pipe of simple, elliptic section and a body of polygonal section that could adapt to a more complex shape through inversion of individual vertices. Figure 15.11B shows contours of the measured magnetic field and of the closely matching field computed from the polygonal-section model. Also shown in Fig. 15.11B are the plans of the top section of the elliptic-section (blue) and polygonal-section (red) models. Only the polygonal-section model is complex enough to match the detail of the anomaly and it is possible that the two centres of magnetisation revealed by this model might be separate but adjacent bodies. Both models are of limited depth extent as consistent with a tuya, are broadly coincident and have similar magnetisation directions

(Table 15.3) with a difference of only 7°. Figure 15.12 shows a section through the models on the westernmost of the two lines that pass through the anomaly. The section shows the limited depth extent and that the polygonal model has attempted to match the two anomaly peaks with two segments coincident with two topographic peaks.

15.5.4 ARAD anomaly 346, Grange Common, County Kildare, Ireland

Figure 15.13 shows a segment of TMI over Ireland measured in the Tellus Survey nation programme of the Geological Survey of Ireland. The data can be downloaded from Tellus (https://www.gsi.ie/en-ie/programmes-and-projects/tellus/Pages/default.aspx). The section of the survey including anomalies ARAD344 to ARAD346 was flown on north-north-west to south-south-east flightlines at 200 m spacing and a nominal 60 m terrain clearance (variable in the drape over the topography associated with ARAD346). Anomalies ARAD344 and ARAD345 are compact, almost circular negative anomalies apparently due to reversely magnetised volcanic pipes (for magnetisation details see Table 15.3 or download the models from ARAD). Figure 15.14A shows anomaly ARAD346 over a body of Ordovician andesites at Grange Common similar to those exposed in the Hill

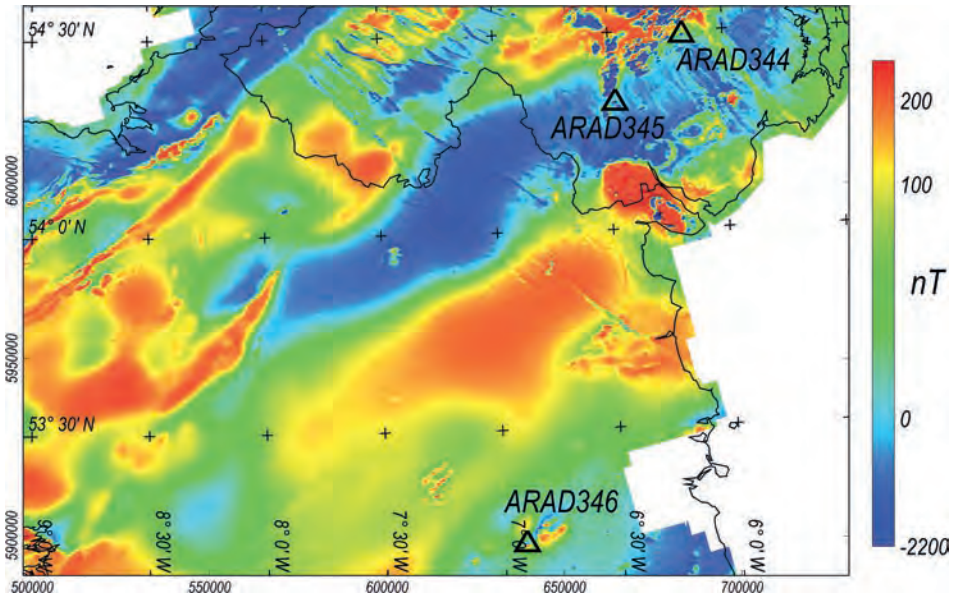

Fig. 15.13. TMI image of a segment of the Tellus Ireland Survey with anomalies ARAD344 to ARAD346.

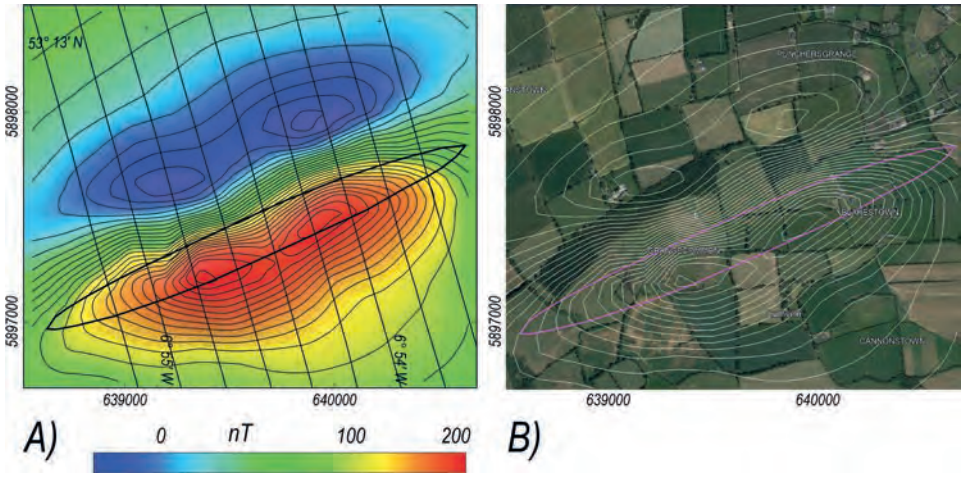

Fig. 15.14. A) TMI anomaly ARAD346 with flightlines and outline of the top surface of the model and B) TMI contours and body outline over a Google Earth image of the area.

of Allen Quarry to the north-east. ARAD346 could be split into two overlapping anomalies but their common pattern suggests that they are (possibly joined) sources of identical or similar magnetisation direction as reported in Table 15.3 (the models can be downloaded from ARAD). A more complex model could improve the match to the input anomaly but would not necessarily increase confidence in the estimated magnetisation direction (the anomaly could also be upward continued to provide data less sensitive to the details of its distribution).

15.5.5 ARAD anomaly 339, Hennock, Devon, UK

Figure 15.15 shows a TMI image from a part of the Tellus SW survey of south-west England (Beamish *et al.* 2014). This is an area with a long and intensive history of metalliferous mining. The survey was flown for the British Geological Survey (BGS) on north–south lines at 200 m spacing and a mean terrain clearance of 91 m. Data can be downloaded from the Tellus South West Project website (https://www.tellusgb.ac.uk/data/airborneGeophysicalSurvey.html). Regional magnetic field variations are subdued over the magnetically quiet Permian Dartmoor and Cornish granites and over the Devonian and Carboniferous sediments they are intruded into, with higher amplitude magnetic field variations over the contact metamorphic regions around the granites and associated with more localised features, including some associated with mineralisation in and around the granites. These more localised magnetic field variations have a wide range of patterns. Three of the anomalies (of broadly consistent pattern) ARAD339 to ARAD341 are located in Fig. 15.15 and their inversion details are reported in Table 15.3. Figure 15.16A shows the easternmost of these three anomalies to the west of Hennock in the Teign Valley. The anomaly is well defined on four to five flightlines and has opposite polarity to that expected of an induced magnetisation. The anomaly peak and trough amplitudes are more similar than would be expected at this steep geomagnetic inclination, suggesting that the magnetisation has a low inclination. The anomaly is closely matched by a simple steeply plunging pipe of elliptic section and predominantly remanent magnetisation (Table 15.3). The plan of the top of the model is shown over the TMI image in Fig. 15.15A and over a Google Earth image of the area in Fig. 15.15B. A section along the central north–south light-line shown in Fig. 15.17 indicates that the body is narrow, steeply dipping and terminates at or close to surface. The anomaly was modelled with both an ellipsoid and an elliptic-section pipe model with almost identical results in locating the magnetisation and determining its direction. The Teign Valley where the anomaly is located has a long history of base metal mining of deposits associated with intrusion of the Dartmoor Granite, with east–west lodes parallel to apparent elongation of the source bodies for the ARAD339 anomaly. The Great Rock Mine that mined

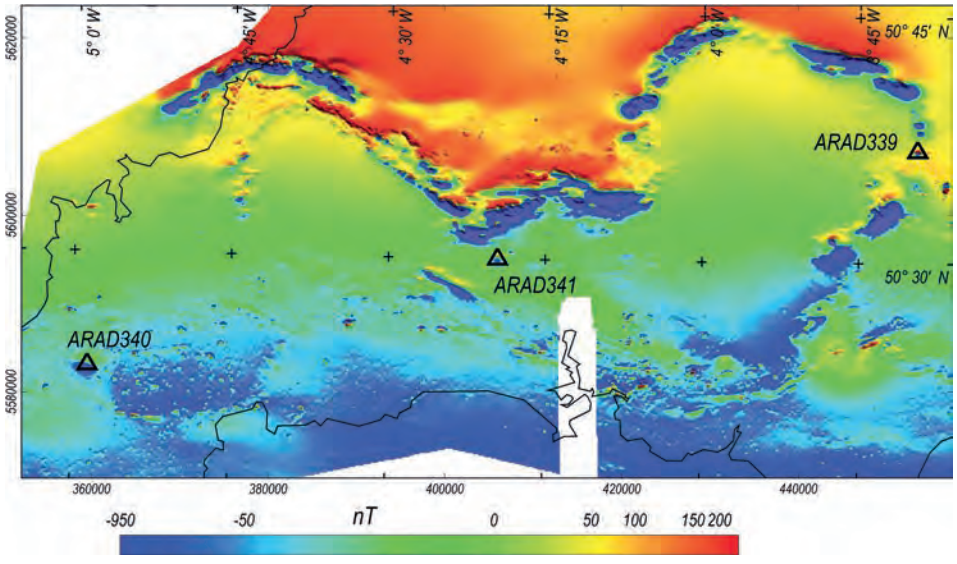

Fig. 15.15. TMI image of a section of the Tellus South-west survey including anomalies ARAD339 to ARAD341.

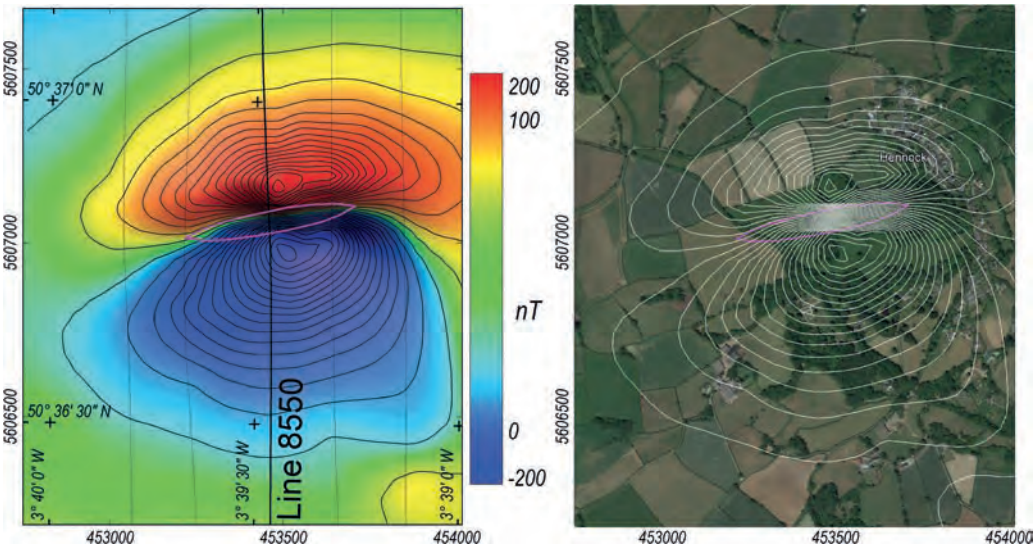

Fig. 15.16. A) TMI anomaly ARAD339 with flightlines and outline of the top surface of the model and B) TMI contours and body outline over a Google Earth image of the area.

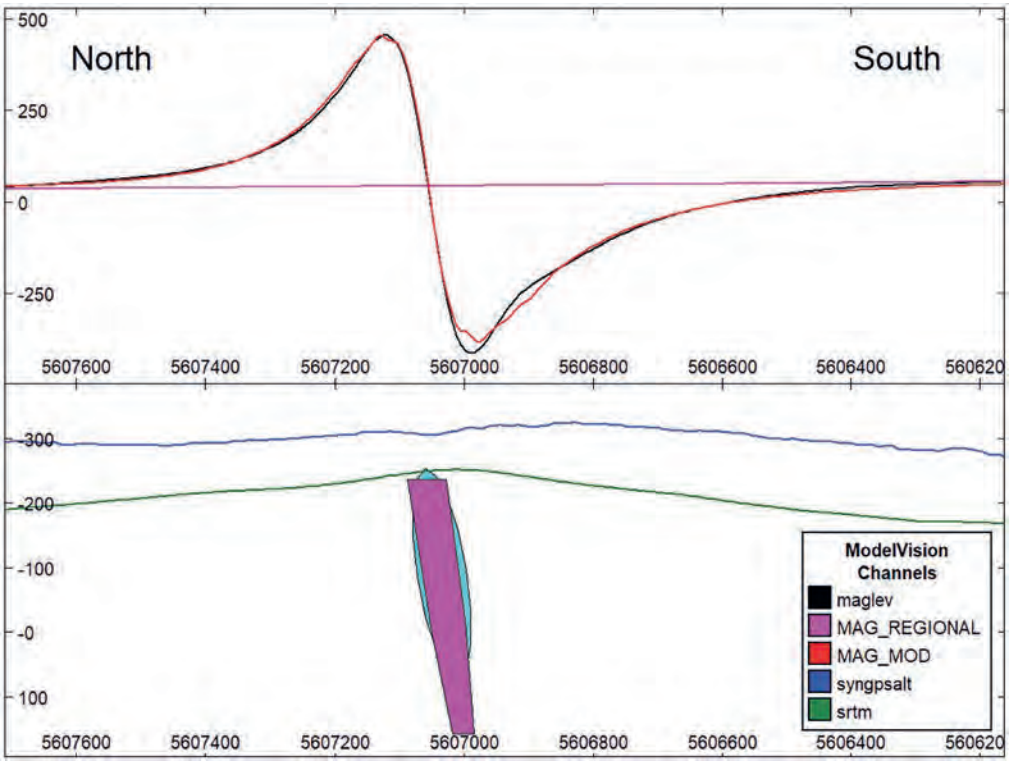

Fig. 15.17. Section along flightline 8550 (for location see Fig. 15.16) with elliptic-section pipe (magenta) and ellipsoid (turquoise) model intersections. The computed field channel is for the elliptic-section pipe model.

micaceous hematite (formerly used to paint the Sydney Harbour Bridge and British warships) is located only 1 km to the north of ARAD339. Two anomalies of similar pattern due to apparently larger and deeper magnetisations, 2 and 3 km to the north of ARAD339 (and visible in Fig. 15.15) might be due to untested mineralisation (but are within the Dartmoor National Park area).

15.5.6 The Haugsbygd anomaly ARAD347, Norway

Figure 15.18 shows a TMI image of Anomaly ARAD347 north of Haugsbygd in the Buskerud Region of Norway, extracted from the 2010 Kroderen heli-magnetic and EM Survey flown by the Geological Survey of Norway on east–west flightlines at 200 m spacing and 75 m terrain clearance. The data can be downloaded from https://www.ngu.no/mins-data/Geofysikk/. The anomaly is well matched by an outcropping or sub-cropping circular-section plunging pipe with a moderate-inclination reverse magnetisation of ARRA 138°. Details of the model magnetisation estimate are listed in Table 15.3 and the model can be downloaded from ARAD. The anomaly and source model are broadly coincident with a topographic high that suggests it may be possible to directly test the magnetisation by sampling of suitable outcrop. The compact anomaly and relatively undeveloped area might make this a suitable site for a lower-level, closely line-spaced drone survey to investigate any complexity of the anomaly unresolved by the currently spare coverage on only four key flightlines.

15.6 EMAG2 DATABASE ENTRIES

Mid- to high-resolution aeromagnetic surveys (line spacings of 500 m and less and terrain clearances of 150 m and less) over shallow magnetisations generally record a population of many small anomalies and progressively fewer large anomalies. The multiple smaller anomalies constitute many of the solutions in the ARAD database but these anomalies attenuate rapidly with height and are either unrepresented or insufficiently sampled by surveys at higher elevation (that generally also have wider line spacing). EMAG2 is a global TMI coverage generated from a composite of many national and regional datasets that are in many cases themselves composites from multiple surveys (https://www.ncei.noaa.gov/products/earth-magnetic-model-anomaly-grid-2). The EMAG2 grid has a cell size of two arc seconds and nominally represents the field at 4 km elevation. It is constructed predominantly from aeromagnetic and marine magnetic ship-track data, with satellite data used for levelling. Validity and resolution of EMAG2 varies with location according to the quality and sufficiency of the input data. At the 4 km elevation the magnetic field is reasonably defined by sparse sampling but the low-elevation input data that are used to derive the high elevation field should be of at least moderate resolution to restrict aliasing before upward continuation. Anomalies in the EMAG2 grid are mostly due to clusters of shallow strong magnetisations (possibly resolved individually in low-elevation magnetic field data) that are broad enough to generate longer wavelength field variations and/or deeper moderate to strong (generally larger volume) magnetisations that in low-elevation magnetic field data are in many cases partially obscured by

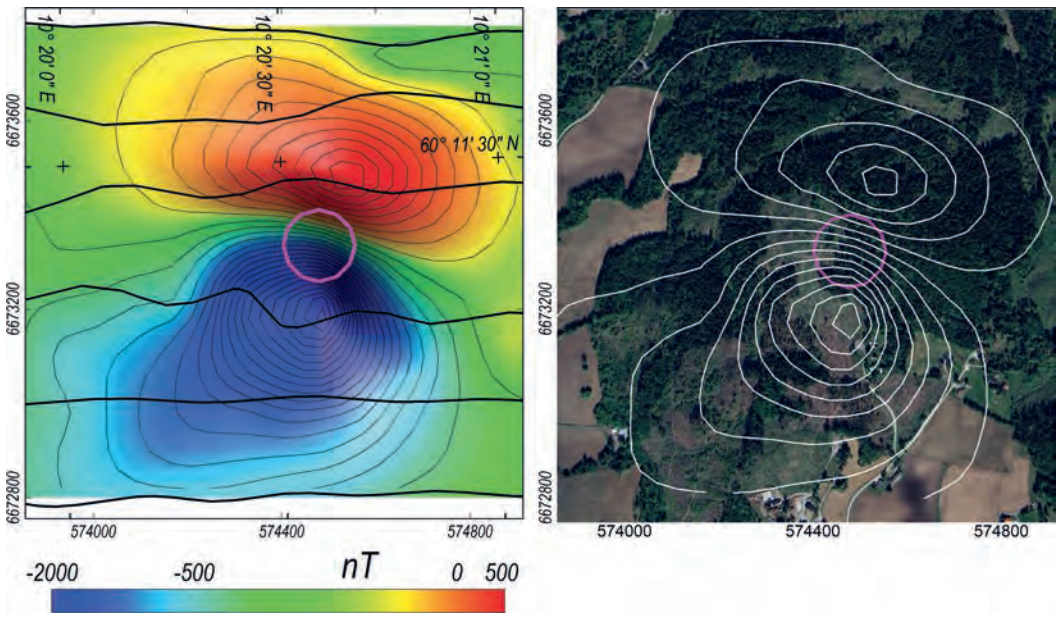

Fig. 15.18. A) ARAD347 TMI anomaly with flightlines and plan of the top of the circular-section pipe model and B) the TMI anomalies and model plan over a Google Earth image.

overprinting short-wavelength field variations of shallow magnetisations. Each anomaly in EMAG2 yields a single magnetisation estimate that is at best representative of the combined magnetisations that generate it. There are undoubtedly also anomalies in EMAG2 that are due to multiple distributed magnetisations for which an estimated magnetisation direction is a factor not just of the contributing (possibly strongly variable) magnetisations but also of their spatial distribution. Nevertheless, EMAG2 provides a valuable resource to estimate large scale magnetisations over regions where input data is of moderate to high quality and suitability but is not easily accessible elsewhere. EMAG2 anomalies in regions where input data are less sufficient or less reliable should be treated with greater caution.

We investigate EMAG2 anomalies in two areas of high-quality input data. We compare magnetisation directions recovered from four prominent EMAG2 anomalies over Mexico with estimates from the anomalies in the North American Magnetic Anomaly Map (https://pubs.usgs.gov/publication/70211067) and in the north-east of Western Australia we compare magnetisation directions derived from EMAG2 anomalies with directions derived from the Australian national TMI grid (https://ecat.ga.gov.au/geonetwork/dashboard/api/records/f2e58161-24cf-42d2-b328-a9039f72113b).

15.6.1 North American Map and EMAG2 anomalies over volcanic intrusions in Mexico

Figure 15.19 shows images of prominent TMI anomalies over volcanic intrusions in Mexico from A) the Magnetic Anomaly Map of North America (MAMNA) at a 1 km elevation and B) from EMAG2 at a 4 km elevation. The EMAG2 data over this region is an upward continuation of the MAMNA grid or of the same input data as for that grid. In the absence of original flightline data it is acceptable to estimate source magnetisation direction from well defined grid anomalies provided there is confidence in the construction of those grids. Derivation of source magnetisation details such as depth to the top of magnetisation is less reliable from grid data (as discussed in Chapter 3). However, as established in Chapters 5 and 6, estimation of mean magnetisation direction from grid data is relatively robust.

A study using data from MAMNA (García-Abdeslem and Calmus 2019) reports a magnetisation direction of declination 5°, inclination 50° for Anomaly ARAD335. Inverting the anomaly for magnetisation direction using elliptic-section pipe and ellipsoid models we obtained directions different to the estimate by García-Abdeslem and Calmus by 20° and 19° respectively and from the equivalent anomaly ARAD348 in the EMAG2 grid (with the same two body types) different by only 4° and 5°.

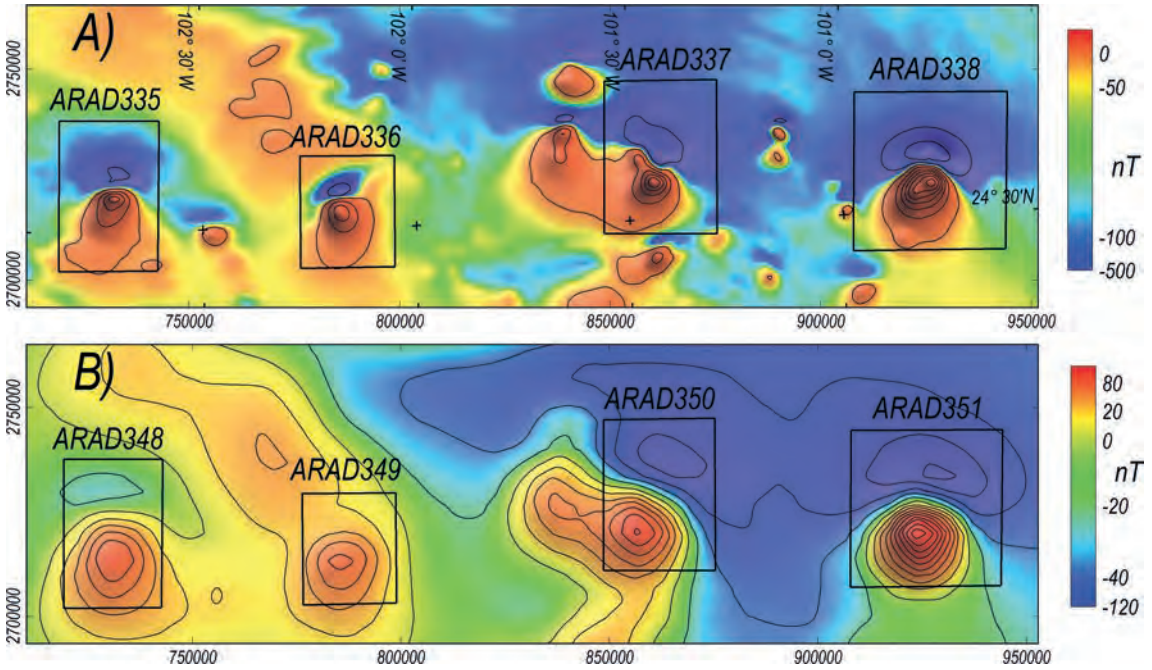

Fig. 15.19. An east–west string of TMI anomalies in Mexico (for location see Fig. 15.4), A) in the North American Magnetic Anomaly Map (elevation 1 km, contour interval 200 nT) and B) in EMAG2 (elevation 4 km, contour interval 20 nT).

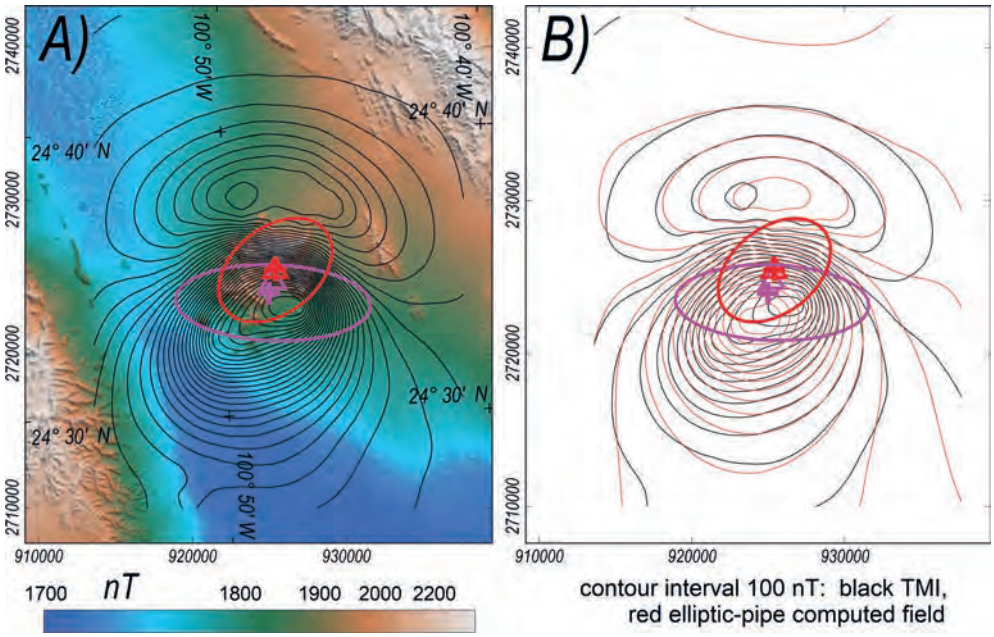

Fig. 15.20. A) contours of ARAD338 from the MAMNA Grid over an image of SRTM and B) those contours (black) and contours of the elliptic-section pipe computed field (red). The top of the elliptic-section pipe models for Anomalies ARAD338 (MAMNA) and ARAD351 (EMAG2) are shown in red and magenta respectively. Crosses mark the centres of the tops of the models and triangles their body centres.

Figure 15.20A shows contours of ARAD338 (the easternmost anomaly in Fig. 15.19B) over an image of SRTM (https://www.usgs.gov/centers/eros/science/usgs-eros-archive-digital-elevation-shuttle-radar-topography-mission-srtm-1). The El Peñuelo intrusive complex (Velasco-Tapia *et al.* 2011) consists of a range of lithologies including monzodiorite and quartz syenite that form a topographic high of 750 m. The range of elevation complicates processing of the MAMNA grid and may persist to influence the EMAG2 grid at higher elevation. The tops of the elliptic-pipe source models from inversion of the MAMNA and EMAG2 data shown in Fig. 15.20 are different but overlap considerably. The centre-points of the tops of the bodies differ by 1,560 m, only one-half of the EMAG2 cell size. The difference between the magnetisation direction of the two models is only eight degrees (the mean difference for the four pairs of anomalies is 9°). For all four pairs of anomalies there is a better fit of the computed fields to the higher and simpler EMAG2 anomalies than to the more complex lower-elevation MAMNA anomalies, but we consider inversion of the lower elevation data to be more reliable because of the higher anomaly amplitudes and more distinct separation from background fields.

15.6.2 EMAG2 anomalies over strong magnetisation in north-east Western Australia

Figure 15.21 shows images of high-amplitude TMI variations in north-east Western Australia: A) from the national Australian TMI grid and B) from EMAG2. Figure 15.22A shows TMI contours in the Australian national grid for the area of Anomaly ARAD354. There is a range of 36,000 nT in a background field of just less than 52,000 (the contour interval in Fig. 15.22A is 1,000 nT). This extreme magnetic field variation causes local rotation of the geomagnetic field that invalidates various transforms of the data. Modelling of the data through computation of orthogonal field components is not susceptible to this problem but the extreme field variations raise a series of challenges in data acquisition and processing. In consequence the models are of lower reliability than models of more moderate magnetisations. These magnetic field anomalies coincide with regions of (sparse) outcrop of the banded and folded Nimingarra Iron Formation, a basal unit of the Archaean Pilbara Supergroup. The extreme magnetisations giving rise to these high-amplitude anomalies include considerable self-demagnetisation effects and most probably significant anisotropy of magnetic

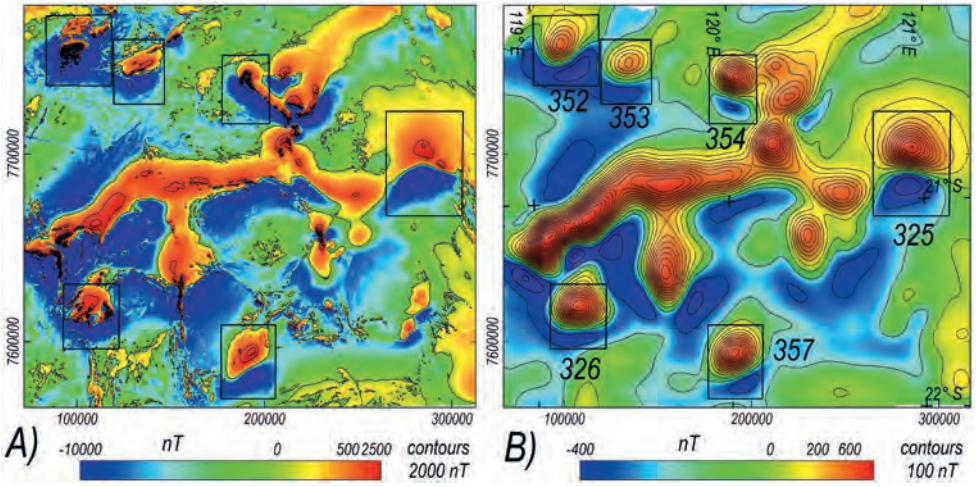

Fig. 15.21. TMI images over north-east Western Australia A) from the national Australian TMI grid and B) from EMAG2.

susceptibility as well as complex remanent magnetisations (magnetisations of the nearby similar Hammersley iron formation are described by Clark and Schmidt 1994 and Guo 2015). In consequence, the effective magnetisation estimated from modelling of the anomalies does not directly represent magnetisations that would be measured on rock samples in the laboratory.

To compare anomalies in the Australian national grid and EMAG2 we directly inverted the Australian national grid data using 14 plunging elliptic-section pipe bodies, each assigned to explain discrete peaks in TMI (more reliable details could be obtained from inverting the primary survey flightline data). Each body was allowed free resultant magnetisation direction. The field computed from the assemblage of bodies matches the input field closely (Fig. 15.22A) but the overlap of adjacent anomalies reduces confidence in their individual parameter values. The mean magnetisation direction for the model was estimated by vector summation of the magnetisation directions weighted by the product of

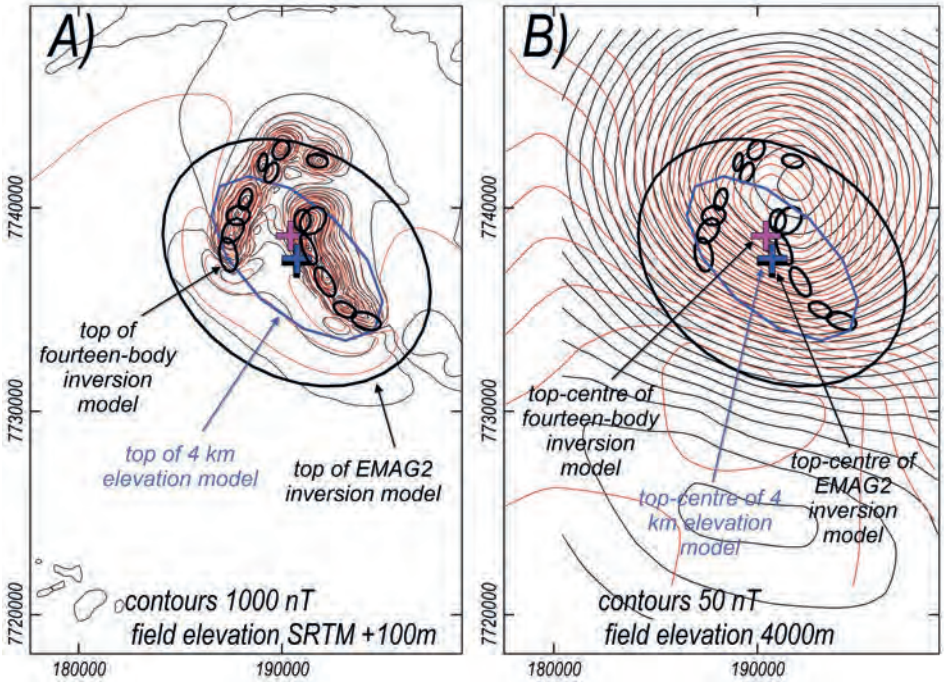

Fig. 15.22. A) contours of the Australian national TMI grid (black) and of the field computed from the 14 elliptic-section pipe model (red) and B) contours of the EMAG2 ARAD354 anomaly (black) and of the field at 4 km elevation computed from the 14-body model (red).

magnetisation-intensity and area of the top of the bodies, and separately by the product of magnetisation-intensity and volume. These two mean directions (listed in Table 15.4) differ by only 2°. The mean difference of the individual body magnetisation directions from the population mean directions was in both cases 13°. We do not know to what extent this range of magnetisation direction represents true variation in magnetisation direction or error in its estimation.

We computed the field from this 14-body model at an elevation of 4 km for comparison with the EMAG2 grid. The EMAG2 contours (black) and model-computed contours (red) are shown in Fig. 15.22B. These two grids, derived in very different ways are broadly similar but differ in detail. We inverted both the EMAG2 anomaly (Anomaly ARAD354) and the field of the 14-body model computed at the same 4 km elevation, in each case using single plunging elliptic-section pipe models. Magnetisation parameters of these inversion models are reported in Table 15.4. The difference in recovered magnetisation direction estimates from the two inversions is only 4°. The difference in magnetisation direction between the 14-body model and the single-body inversion of its field at 4 km is 13°. The top surface of the elliptic-section pipe model inverted from the 14-body model field is plotted in Fig. 15.22A and Fig. 15.22B. Also plotted in Fig. 15.22B are the outline of the elliptic-section pipe model from inversion of the EMAG2 data and the centre points of both single-body inversion models and the 14-body inversion model. The

Table 15.4. Magnetisation details for models from inversion the EMAG2 ARAD354 anomaly, of the equivalent anomaly in the Australian national TMI grid (the '14-body' model), and of the field of the 14-body model computed at an elevation of 4 km.

Model	Elevation m	Volume km^3	Intensity A/m	Magnetic moment $A.m^2.10^{12}$	Declination degrees	Inclination degrees
Fourteen-body weighted by top surface	100				71	-73
Fourteen-body weighted by volume	100	28.24	74.2	2.1	78	-74
Single-body inversion of 14-body field	4,000	249	9.8	2.4	132	-80
EMAG2	4,000	1,668	9.4	15.7	130	-76

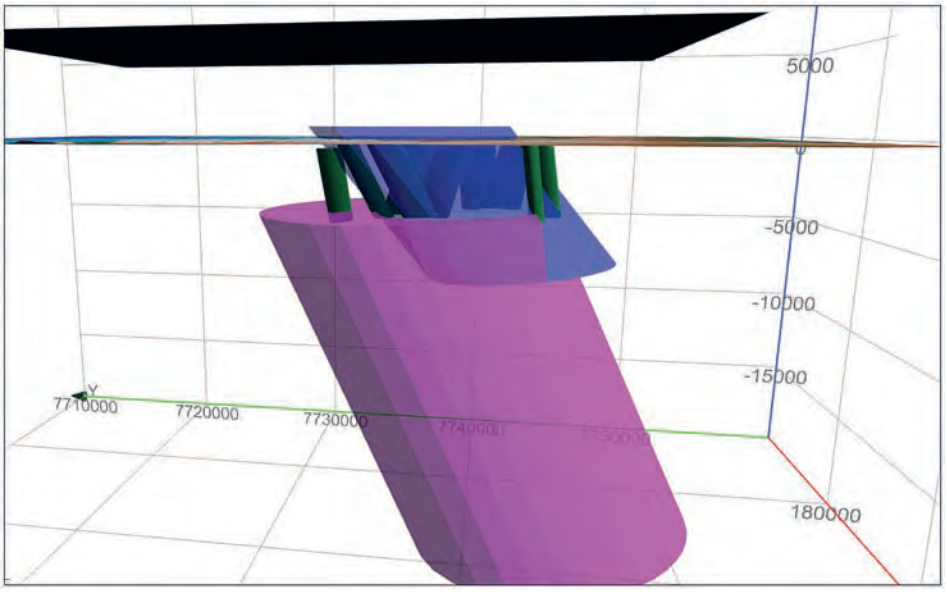

Fig. 15.23. Perspective view of the EMAG2 inversion model (magenta), 14-body Australian national TMI grid inversion model (green) and the body from inversion of the 14-body field computed at 4 km elevation (blue).

two models from inversion of the data at 4 km elevation that have magnetisation differences of only 4° have top-surface centres different by only 200 m compared to the separation of 1250 m to the top-centre of the 14-body model that has a difference in magnetisation direction of 13°.

Figure 15.23 shows the three inversion models in perspective view. Although the horizontal centres of the tops of these models and their magnetisation directions are similar, their other spatial details vary considerably. Note that the 14-body model and single-body inversion model, shown in green and blue respectively in Fig. 15.23, produce near-identical fields at the elevation of 4 km although they are very different distributions of magnetisation. The EMAG2 inversion model (in magenta) that produces only a slightly different magnetic field (see Fig. 15.22B) has very different depths to its top and base, with only minor overlaps with the other models.

This study is at a different scale to most magnetic field inversions performed in mineral exploration (and in investigation of most of the much smaller anomalies in ARAD) but it highlights some common features: that spatial detail of the distribution of magnetisation can only be resolved in proximal fields, that inversion of distal fields generally only justifies simple models of homogeneous magnetisation, and that (mean) magnetisation direction and horizontal centre of the top of magnetisation are the more reliable results recovered from magnetic field inversion.

15.7 CONCLUSIONS

We have discussed the design and implementation of the Australian remanent anomalies database and suggest that this database or its blueprint could usefully be applied to establish a global database or linked databases to resolve and integrate magnetisation directions derived from analysis and inversion of magnetic field data with palaeomagnetic and rock magnetic studies at regional, national and global scales. In this publication we present a range of solutions from beyond Australia, similarly derived from FAIR data made available by national geological surveys. We also include study of anomalies from the EMAG2 global magnetic field grid, selected to illustrate the capabilities and limitations of investigating magnetisation at larger scale and greater elevation.

REFERENCES

Beamish D, Howard AS Ward EK White J Young ME (2014) 'Tellus South West airborne geophysical data.' Natural Environmental Research Council, British Geological Survey.

Briggs IC (1974) Machine contouring using minimum curvature. *Geophysics* **39**, 39–48. doi:10.1190/1.1440410

Clark DA (2014) Methods for determining remanent and total magnetisations of magnetic sources – a review. *Exploration Geophysics* **45**, 271–304. doi:10.1071/EG14013

Clark DA, Schmidt PW (1994) Magnetic properties and magnetic signatures of BIFS of the Hamersley Basin and Yilgarn Block, Western Australia. *Exploration Geophysics* **25**, 169. doi:10.1071/EG994169a

Dannemiller N, Li Y (2006) A new method for determination of magnetization direction. *Geophysics* **71**, L69–L73. doi:10.1190/1.2356116

Davis A (2022) Nested anisotropic geostatistical gridding of airborne geophysical data. *Geophysics* **87**, E1–E12. doi:10.1190/geo2021-0169.1

Fedi M, Florio G, Rapolla A (1994) A method to estimate the total magnetization direction from a distortion analysis of magnetic anomalies. *Geophysical Prospecting* **42**, 261–274. doi:10.1111/j.1365-2478.1994.tb00209.x

Foss CA, McKenzie KB (2011) Inversion of anomalies due to remanent magnetisation: an example from the Black Hill Norite of South Australia. *Australian Journal of Earth Sciences* **58**, 391–405. doi:10.1080/08120099.2011.581310

García-Abdeslem J, Calmus T (2019) The monzonitic to dioritic pluton of Cerro Prieto, Durango, Mexico: a Larimide laccolith inferred by nonlinear 3D inversion of aeromagnetic data. *Journal of Applied Geophysics* **160**, 121–130. doi:10.1016/j.jappgeo.2018.10.026

Gerovska D, Araúzo-Bravo MJ, Stavrev P (2009) Estimating the magnetization direction of sources from southeast Bulgaria through correlation between reduced-to-the-pole and total magnitude anomalies. *Geophysical Prospecting* **57**, 491–505. doi:10.1111/j.1365-2478.2008.00761.x

Guo WW (2015) Magnetic mineralogical characteristics of Hamersley iron ores in Western Australia. *Zeitschrift für Angewandte Mathematik und Physik* **3**, 150–155. doi:10.4236/jamp.2015.32023

Helbig K (1963) Some integrals of magnetic anomalies and their relation to the parameters of the disturbing body. *Zeitschrift für Geophysik* **29**, 83–96.

Irving E (1964) 'Palaeomagnetism and its application to geological and geophysical problems' Wiley, 399 pages.

Jarboe NA, Koppers AA, Tauxe L, Minnett R, Constable C (2012) 'The online MagIC Database: data archiving, compilation, and visualization for the geomagnetic, paleomagnetic and rock magnetic communities' In: Abstract GP31A–1063, AGU Fall Meeting.

Li J, Zhang Y, Yin G, Fan H, Li Z (2017) An approach for estimating the magnetization direction of magnetic anomalies. *Journal of Applied Geophysics* **137**, 1–7. doi:10.1016/j.jappgeo.2016.12.009

Liu S, Hu X, Zhang D, Wei B, Geng M, Zuo B, Zhang H, Vatankhah S (2020) The IDQ curve: a tool for evaluating the direction of remanent magnetization from magnetic anomalies. *Geophysics* **85**(5), J85–J98. doi:10.1190/geo2019-0545.1

McElhinny MW (1973) 'Palaeomagnetism and plate tectonics (Earth Science Series)' Cambridge University Press, New York, 368 pages.

Naprstek T, Smith RS (2019) A new method for interpolating linear features in aeromagnetic data. *Geophysics* **84**, JM15–JM24. doi:10.1190/geo2018-0156.1

Phillips JD (2005) Can we estimate total magnetization directions from aeromagnetic data using Helbig's integrals? *Earth, Planets, and Space* **57**, 681–689. doi:10.1186/BF03351848

Pisarevsky SA (2005) New edition of the Global Paleomagnetic Database. *Eos (Washington, D.C.)* **86**(17), 170. doi:10.1029/2005EO170004

Pisarevsky SA, McElhinny MW (2003) Global Paleomagnetic Data Base developed into its visual form. *Eos (Washington, D.C.)* **84**(20), 192. doi:10.1029/2003EO200007

Pisarevsky SA, Li ZX, Tetley MG, Liu Y, Beardmore JP (2022) An updated internet-based global palaeomagnetic database. *Earth-Science Reviews* **235**, 1–14. doi:10.1016/j.earscirev.2022.104258

Pratt DA, White AS, Parfrey KL, McKenzie KB (2020) 'ModelVision User Guide Version 17.0' Tensor Research Pty Ltd. ModelVision 17.5 User Guide (tensor-research.com.au).

Schmidt PW (2014) A review of Precambrian palaeomagnetism of Australia: palaeogeography, supercontinents, glaciations and true polar wander. *Gondwana Research* **25**(3), 1164–1185. doi:10.1016/j.gr.2013.12.007

Schmidt PW, Clark DA (2000) 'Paleomagnetism, apparent polar-wander path, & paleolatitude'. In: *Billion-year Earth History of Australia and Neighbours in Gondwanaland*. (Ed. JJ Veevers) pp. 12–17. Gemoc Press.

Schmidt PW, Powell CM, Li ZX, Thrupp GA (1990) Reliability of Palaeozoic palaeomagnetic poles and APWP of Gondwanaland. *Tectonophysics* **184**(1), 87–100. doi:10.1016/0040-1951(90)90122-O

Staisch LM, Connell DM, Blakely RJ (2024) High-Resolution Airborne magnetic and radiometric survey of the Republic Graben, Okanogan and Kettle Metamorphic core complexes, Kootenay Arc and surrounding regions, Northeastern Washington. U.S. Geological Survey data release. doi:10.5066/P1PKEZOJ

Stavrev P, Gerovska D (2000) Magnetic field transforms with low sensitivity to the direction of source magnetization and high centricity. *Geophysical Prospecting* **48**, 317–340. doi:10.1046/j.1365-2478.2000.00188.x

Velasco-Tapia F, González-Guzmán R, Chávez-Cabello G, Lozano-Serna J, Valencia-Moreno M (2011) Estudio petrográfico y geoquímico del Complejo Plutónico El Peñuelo (Cinturón de Intrusivos de Concepción del Oro), noreste de Mexico. *Bulletin of the Geological Society of Mexico* **63**, 183–199. doi:10.18268/BSGM2011v63n2a4